Magnetic orders induced by RKKY interaction in Tsai-type quasicrystalline approximant Au-Al-Gd

Haruka Miyazaki, Takanori Sugimoto,* Katsuhiro Morita,† and Takami Tohyama
Department of Applied Physics, Tokyo University of Science, Katsushika, Tokyo 125-8585, Japan

(Received 29 November 2019; accepted 14 February 2020; published 28 February 2020)

Recent experimental study on the Tsai-type quasicrystalline approximant Au-Al-Gd, which is a crystal but has the same local structure as quasicrystals, has revealed the presence of magnetic orders and phase transitions with changing the Au/Al concentration. Motivated by the experiment, we theoretically investigate whether a successive change of magnetic orders occurs in a minimal magnetic model including the Ruderman-Kittel-Kasuya-Yosida (RKKY) interaction only. We find that the model induces multifarious magnetic orders depending on the Fermi wavenumber and gives a good starting point for understanding the experimental observation. In addition, we predict the presence of an undiscovered magnetic order called cuboc order at the large Fermi wavenumber region.

DOI: 10.1103/PhysRevMaterials.4.024417

I. INTRODUCTION

Recent experimental studies on Tsai-type quasicrystals including rare-earth ions [1,2] have successively provided startling discoveries of novel phenomena: valence fluctuation [3,4], quantum criticality [5,6], and superconductivity [7,8]. These phenomena are induced by strongly correlated electrons originating from rare-earth ions, particularly Yb and Ce. The physics behind the phenomena might be similar to that of heavy-fermion materials. However, there would be other exotic phenomena originating from the quasiperiodicity or peculiar local structures of quasicrystals in spite of recent theoretical efforts [9–13].

Tsai-type quasicrystalline approximants, which have the same local structure as quasicrystals but keep the translational symmetry [14], have also attracted much attention due to the experimental discovery of various magnetic orders [15], e.g., ferromagnetism, antiferromagnetism, and spin-glass-like magnetism, both in binary [16–20] and ternary [21–28] compounds. This is in contrast to quasicrystals where there is no report on magnetic order so far [29–37]. In the approximants, the magnetic moments located on rare-earth ions can interact with each other via the Ruderman-Kittel-Kasuya-Yosida (RKKY) interaction [38–40]. Atomic composition in the approximants is a controlling parameter of the Fermi wavenumber k_F, which changes spatial extension of the RKKY interaction. Therefore, an idea that the RKKY interaction as a function of k_F is crucial for understanding the various magnetic orders has been put forward [15]. However, the crystal structure of Tsai-type quasicrystals and approximants is too complicated to theoretically analyze the magnetic behaviors. Actually, magnetic orders in three-dimensional quasicrystals and approximants remain unclear from theoretical viewpoints, contrary to pioneering works on magnetism in low-dimensional quasiperiodic systems [41–49].

The Au-Al-Gd system is one of 1/1 Tsai-type quasicrystalline approximant Au-X-R (X = Al, Si; R = Gd, Tb, Ho, Dy) showing magnetic orders [22,26,50]. With increasing Au concentration, i.e., decreasing k_F, magnetism in Au-Al-Gd changes from spin glass to ferromagnetism and to antiferromagnetism [24,26]. Since single-ion anisotropy due to spin-orbit coupling and crystal field is weak on a Gd ion, the Au-Al-Gd system is a good material to investigate the interplay of RKKY interactions and the complicated structure in the Tsai-type approximants.

In this paper, we theoretically investigate magnetic states in Au-Al-Gd based on the classical approximation of localized quantum spins on Gd ions. The approximation is justified by the facts that (i) the magnetic moment on Gd ions has been estimated to be $\mu_{\rm eff} = 8.74\mu_B$ from magnetic susceptibility [24,26] (cf. that the effective moment of a single Gd^{3+} ion is $7.94\mu_B$), which is large enough to be approximated as a classical spin, and (ii) magnetic properties in a Tsai-type 1/1 approximant Au-Si-Tb with the same crystal structure as Au-Al-Gd but with strong single-ion anisotropy [20,27] have been described well by the classical approximation [50]. Calculating possible magnetic orders in a simple model with both Gd ions in the Tsai-type 1/1 approximant structure and RKKY interaction, we confirm a good qualitative accordance with the experimental change of magnetic orders [24,26]. In addition, we predict an undiscovered magnetic order called cuboc order at the large-k_F region.

The contents of this paper are as follows. In Sec. II, we introduce a minimal model Hamiltonian describing magnetism in the Tsai-type 1/1 approximant Au-Al-Gd with the RKKY interaction. To obtain magnetic ground states, we have performed classical Monte Carlo calculations. Details of the calculations are mentioned in Sec. II. In Sec. III, we present the numerical results and define several order parameters to classify magnetic phases. Additionally, in Sec. IV, we show other phase transitions determined by energy derivative and phase diagram with Curie-Weiss temperature. In Sec. V, we

*sugimoto.takanori@rs.tus.ac.jp
†Present address: Department of Basic Science, University of Tokyo, Meguro, Tokyo 153-8902, Japan.

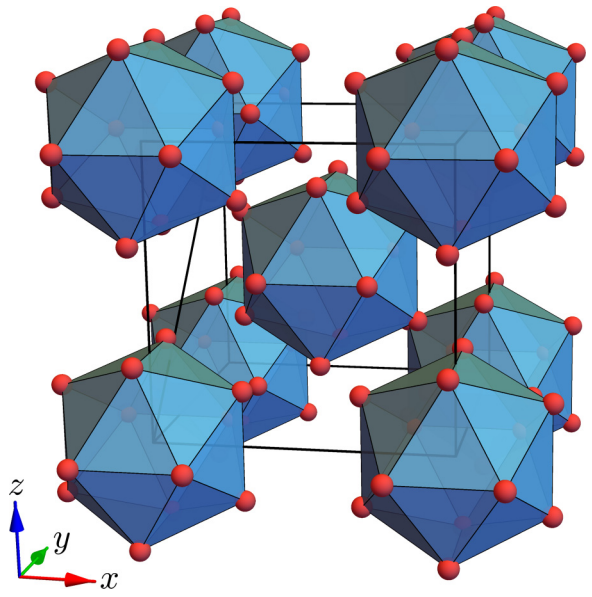

FIG. 1. Magnetic lattice of the Au-Al-Gd alloy. Red spheres denote Gd ions on vertices of an icosahedron. The icosahedra have bcc structure.

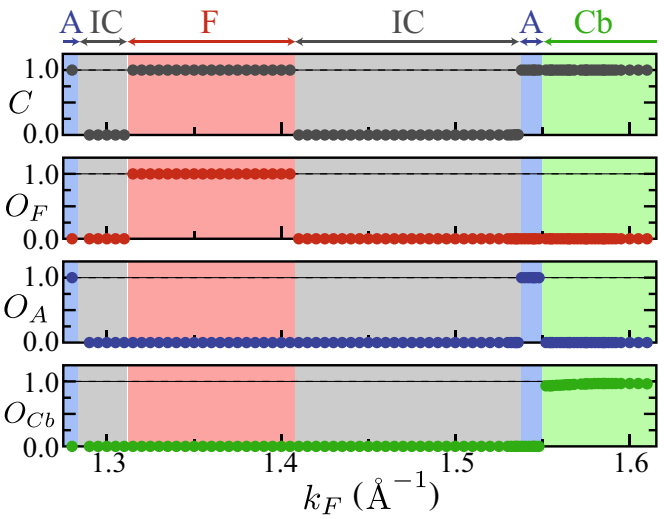

FIG. 2. Phase diagram of Hamiltonian (1) at zero temperature. Four panels represent commensurability C, ferromagnetic order O_F, antiferromagnetic order O_A, and cuboc order O_{Cb}, as a function of the Fermi wavenumber k_F. Color-shaded regions denote commensurate phases, where only one of the order parameters O_F, O_A, or O_{Cb} is finite: the ferromagnetic (F) phase in the red region, the antiferromagnetic (A) phase in the blue region, and the cuboc (Cb) phase in the green region. The gray region corresponds to the incommensurate (IC) phase.

also discuss inconsistencies in the experimental result of Au-Al-Gd. Finally, we summarize our results in Sec. VI.

II. MODEL AND METHOD

A unit cell in the 1/1 approximant includes two Tsai clusters. Gd ions occupy icosahedral vertices of the Tsai cluster. The lattice of Gd ions corresponds to body-centered cubic (bcc) of icosahedra (see Fig. 1), and the localized magnetic moments are located on the Gd ions. Thus, there are 24 spins ($n_s = 24$) in the unit cell.

The minimum model Hamiltonian with the RKKY interaction only is given by

$$\mathcal{H} = -\sum_{|\boldsymbol{r}-\boldsymbol{r}'|<R_c} J_{|\boldsymbol{r}-\boldsymbol{r}'|}\boldsymbol{S}_{\boldsymbol{r}}\cdot\boldsymbol{S}_{\boldsymbol{r}'}, \tag{1}$$

where the exchange energy between two spins, $\boldsymbol{S}_{\boldsymbol{r}}$ at $\boldsymbol{r}$ and $\boldsymbol{S}_{\boldsymbol{r}'}$ at $\boldsymbol{r}'$, is given by $J_{|\boldsymbol{r}-\boldsymbol{r}'|} = Jf(2k_F|\boldsymbol{r}-\boldsymbol{r}'|)$ $(J>0)$ with the function of Friedel oscillation $f(x) = (-x\cos x + \sin x)/x^4$. In this work, we use a classical approximation of quantum spin and thus $\boldsymbol{S}_{\boldsymbol{r}}$ is expressed as a three-dimensional normalized vector with $\|\boldsymbol{S}_{\boldsymbol{r}}\| = 1$. In the 1/1 approximant Au-Al-Gd, the magnetic phases successively change with changing the Au concentration [24,26]. Here we assume that the Fermi wavenumber k_F is determined by the electron density n associated with the Au concentration via $k_F = (3\pi^2 n)^{1/3}$. In Hamiltonian (1), we introduce a cutoff range R_c of the RKKY interaction for simplicity of calculation.

We perform numerical calculation with the classical Monte Carlo (MC) method to obtain spin configurations at zero temperature. In this calculation, we use a single-update heat-bath method combined with the over-relaxation technique and the temperature-exchange method. The system size is set to $N_c = 8\times8\times8$ unit cells, corresponding to $N_s = N_c n_s = 12\,288$ spins, with periodic boundary condition. We take the number of replicas $N_R = 200$, the number of MC steps for relaxation $N_{\mathrm{MC}} = 2400$, and the lowest temperature $T_M/J = 10^{-7}$. After performing the MC simulation, we update the state until the energy converges at $T = 0$ to obtain the ground state. We use $R_c = 50$ Å, which is larger than three times as long as the lattice unit $a = 14.7$ Å [51]. k_F is changed from 1.28 to 1.61 Å^{-1}, where the experimentally determined k_F in Au-Al-Gd is included [24,26].

III. NUMERICAL RESULTS AND ORDER PARAMETERS

To classify spin configurations of the ground state using our method, we consider commensurability defined by

$$C = \frac{1}{n_s}\sum_i \|\langle\boldsymbol{S}_i\rangle\| \tag{2}$$

with the averaged magnitude of spins $\langle\boldsymbol{S}_i\rangle$ over all unit cells: $\langle\boldsymbol{S}_i\rangle = N_c^{-1}\sum_j \boldsymbol{S}_{i,j}$, where $\boldsymbol{S}_{i,j}$ represents the ith spin in the jth unit cell. If spin configuration is invariant with respect to translation of the lattice, the commensurability equals unity. It should be noted that the commensurability is zero in the case of two sublattice configurations; e.g., a spin in a unit cell is directed opposite to the corresponding spin in neighboring unit cells. Thus, this quantity is a measure of ferroic character in the spin configuration. The top panel in Fig. 2 shows the commensurability C as a function of k_F. The value of C alternates between 1 and zero from $k_F = 1.28$ to 1.61 Å; that is, the magnetic state switches from commensurate to incommensurate states and vice versa several times in this region.

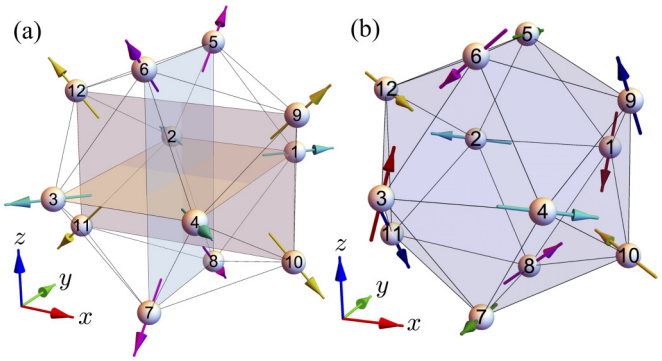

FIG. 3. Cuboc order. (a) An example of spin configuration with $O_{Cb} = 1$. Each plane has four spins denoted by the same color; e.g., the first to fourth spins belong to the xy plane. Neighboring spins in the same plane exhibit 90° order. (b) Spin configuration observed in the MC calculation with $k_F = 1.60$ Å^{-1}. The spin configurations in (a) and (b) are equivalent under a global $O(3)$ rotation.

To clarify the commensurate state in detail, we consider ferromagnetic and antiferromagnetic order parameters defined by

$$O_F = \frac{1}{n_s}\left\| \sum_i \langle \boldsymbol{S}_i \rangle \right\|, \tag{3}$$

$$O_A = \frac{1}{n_s}\left\| \left(\sum_{i\in \mathrm{CCI}} \langle \boldsymbol{S}_i \rangle - \sum_{i\in \mathrm{BCI}} \langle \boldsymbol{S}_i \rangle \right) \right\|, \tag{4}$$

respectively, where CCI (BCI) represents the set of positions on the cubic-cornered icosahedron (body-centered icosahedron) in the unit cell. The second and third panels in Fig. 2 show these order parameters. We find that these order parameters are equal to zero or 1 in the whole region. $O_F = 1$ represents perfect ferromagnetism, while $O_A = 1$ represents an antiferromagnetic phase with Néel order where spins in an icosahedron exhibit ferromagnetic order while spins located in a neighboring icosahedron have the opposite direction. Antiferromagnetic phases are located in narrow regions in Fig. 2.

In Fig. 2, there is a commensurate region with neither ferromagnetic nor antiferromagnetic order above $k_F = 1.55$ Å^{-1}. In the bottom panel of Fig. 2, we successfully identify this magnetic phase with so-called *cuboc* order using a corresponding order parameter [52–54] as follows:

$$O_{Cb} = |\langle \boldsymbol{K}_{xy} \rangle \cdot \langle \boldsymbol{K}_{yz} \rangle \times \langle \boldsymbol{K}_{zx} \rangle| \tag{5}$$

with the averaged vector chirality $\langle \boldsymbol{K}_\alpha \rangle$ of neighboring spins in the $\alpha = xy$, xz, and zx planes given by

$$\langle \boldsymbol{K}_\alpha \rangle = \frac{1}{8} \sum_{\langle i,i' \rangle \in \alpha \text{ plane}} \langle \boldsymbol{S}_i \rangle \times \langle \boldsymbol{S}_{i'} \rangle, \tag{6}$$

where the summation runs over all neighboring bonds $\langle i, i' \rangle$ in the α plane of icosahedron; e.g., $\langle i, i' \rangle = \langle 1, 2 \rangle$, $\langle 2, 3 \rangle$, $\langle 3, 4 \rangle$, and $\langle 4, 1 \rangle$ for the xy plane in Fig. 3. Note that there are two icosahedra in the unit cell, leading to the normalization factor 1/8 in Eq. (6). Supposing a perfect 90° order represented in Fig. 3(a), we obtain $O_{Cb} = 1$. The cuboc order is invariant under a global $O(3)$ rotation of spin configuration. For instance, the spin configuration in Fig. 3(b) obtained by the MC simulation with $k_F = 1.60$ Å^{-1} coincides with the perfect 90° order in Fig. 3(a) by a proper global $O(3)$ rotation.

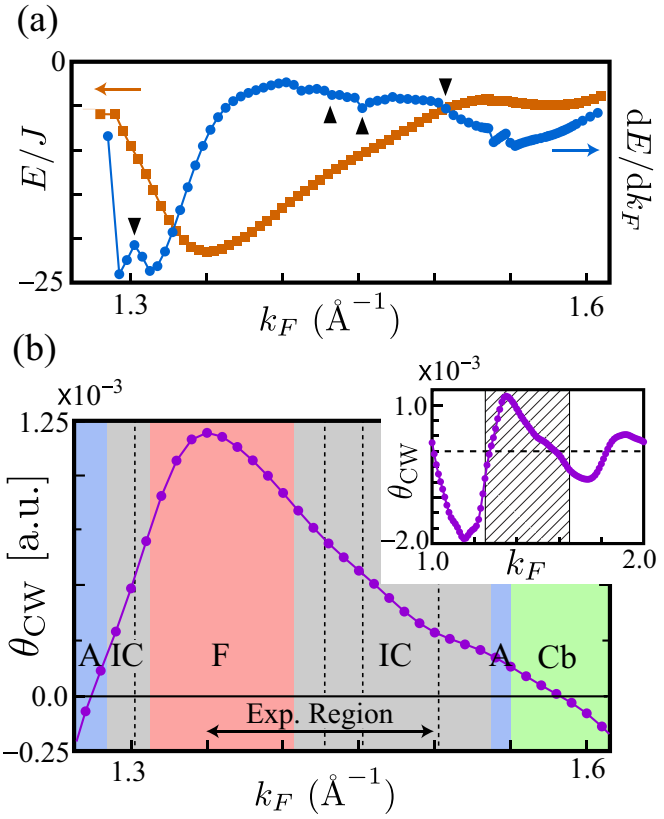

FIG. 4. (a) Total energy of the ground state versus the Fermi wavenumber k_F and its derivative dE/dk_F. In the incommensurate (IC) phases, black triangles denote points where the derivative jumps and cusps indicate the first- and second-order phase transitions, respectively. Other anomalies of the derivative coincide with the phase boundaries obtained in Fig. 2. (b) Curie-Weiss temperature θ_{CW} as a function of $k_F \in [1.25, 1.65]$ Å^{-1}. The inset represents θ_{CW} in a wider region of k_F, where the shaded area corresponds to the simulated region. The vertical dotted lines denote the position of triangles in (a). The ferromagnetic (F), antiferromagnetic (A), cuboc (Cb), and IC phases are taken from Fig. 2. The notation "Exp. Region" indicates a region experimentally investigated [24,26], which is estimated by electron density in the Fermi gas approximation.

IV. PHASE DIAGRAM AND CURIE-WEISS TEMPERATURE

To confirm phase boundaries determined by the order parameters, we calculate the total energy E as a function of k_F and its derivative dE/dk_F as shown in Fig. 4(a). We find clear jumps in dE/dk_F at two antiferromagnetic-incommensurate boundaries with $k_F = 1.29$ Å^{-1} and 1.535 Å^{-1} and at a antiferromagnetic-cuboc boundary with $k_F = 1.55$ Å^{-1}, indicating the first-order phase transition. At two incommensurate-ferromagnetic boundaries with $k_F = 1.315$ and 1.41 Å^{-1}, there is an anomaly-like cusp corresponding to the second-order phase transition. In addition to the expected anomaly at the phase boundaries determined by the order parameters, we find several anomalies in dE/dk_F within the incommensurate phases in Fig. 4(a)

as denoted by black triangles. These anomalies suggest the presence of internal magnetic structures inside the incommensurate phase, which have not been detected by the order parameters examined above. Although detailed study on the internal structures remains as a future work, we have tentatively analyzed spin configurations in each incommensurate phase and found a tendency toward spiral order whose pitch angle depends on the phases, indicating incommensurability in the thermodynamic limit (see the Appendix).

In order to make clear the physical origin of magnetic phases, we plot the Curie-Weiss temperature $\theta_{\rm CW}$ in Fig. 4(b), which is determined by the sum of total exchange energies $\theta_{\rm CW} = (3N_s)^{-1} \sum_{|\boldsymbol{r}-\boldsymbol{r}'|<R_c} J_{|\boldsymbol{r}-\boldsymbol{r}'|}$ based on high-temperature expansion formalism. The inset in Fig. 4(b) shows an alternation of $\theta_{\rm CW}$ between positive and negative values in the wider range of k_F, coming from the oscillating nature of the RKKY interaction. We find that a ferromagnetic phase appears when $\theta_{\rm CW}$ is positively large as expected. On the contrary, antiferromagnetic phases emerge near $\theta_{\rm CW} \cong 0$. This indicates that the antiferromagnetic state composed of ferromagnetic order inside an icosahedral cluster and antiferromagnetic spin arrangement between the neighboring clusters is achieved when the magnitude of intracluster ferromagnetic interactions is comparable to that of intercluster antiferromagnetic interactions. The cuboc phase also appears when $\theta_{\rm CW} \cong 0$, indicating that ferromagnetic and antiferromagnetic interactions are totally canceled out by each other but there is strong frustration as evidenced from 90° order. The incommensurate phase also needs strong frustration, where partial antiferromagnetic interactions may play a key role (see the Appendix).

V. DISCUSSION

Let us compare the calculated phases with experimentally observed ones in the Au-Al-Gd approximant. The experimental data have shown the change of phases from antiferromagnetic to ferromagnetic and to spin-glass phases with increasing k_F [24,26]. The region of experimentally determined k_F based on the Fermi gas approximation is denoted in Fig. 4(b) by "Exp. Region." In the region, however, our calculated phases are only ferromagnetic and incommensurate phases. Therefore, we have two inconsistencies: (i) the antiferromagnetic phase observed in the experiment does not exist in the region and (ii) the spin-glass phase is not obtained in our calculation.

We speculate that the inconsistencies could be explained by the effect of randomness due to chemical disorders and defects in real Au-Al-Gd alloys. First, the randomness will shorten the mean free path of conduction electrons, and thus the cutoff range of the RKKY interaction, R_c, would be shorter than the assumed $R_c = 50$ Å. The shortened cutoff range suppresses the absolute value of the Curie-Weiss temperature $\theta_{\rm CW}$ and shifts the peak of $\theta_{\rm CW}$ at $k_F = 1.35$ Å^{-1} in Fig. 4(b) to larger k_F (not shown). The change of $\theta_{\rm CW}$ can narrow the ferromagnetic phase and may shift it to larger k_F, accompanied by the shift of antiferromagnetic phase around $k_F = 1.30$ Å^{-1} possibly to the estimated experimental region. This will explain inconsistency (i). The randomness may also explain inconsistency (ii) about the absence of a spin-glass state in our result. In general, a spin-glass state is induced by not only frustration but also randomness. Since the incommensurate state in our phase diagram is expected to originate from strong frustration as discussed above, including randomness in our model would bring a spin-glass behavior in cooperation with strong frustration in a certain range of incommensurate phase. This is one of the possible explanations of inconsistency (ii). However, if so, we unfortunately meet another problem in which experimentally observed $\theta_{\rm CW}$ is negative in the spin-glass phase [26] in contrast to the calculated positive $\theta_{\rm CW}$ in our incommensurate phase. In order to resolve this new problem, we may need treat the anisotropy of the crystal field around Gd ions, inhomogeneity of chemical disorders, and magnetic dipole-dipole interactions as precisely as possible. This remains an important problem to be solved in the future.

VI. SUMMARY

We have theoretically investigated magnetic phases in the Tsai-type quasicrystalline approximant Au-Al-Gd alloy using a minimal magnetic model including the RKKY interaction only. The change of Au/Al concentration in the alloy is assumed to correspond to the change of the Fermi wavenumber in our model. Classical MC calculations have been performed to obtain spin configurations at zero temperature. We have found a successive change among antiferromagnetic, ferromagnetic, and incommensurate phases. At large Fermi wavevector, which the real Au-Al-Gd alloy has not reached yet, we have discovered a cuboc phase. Recently such a cuboc order attracted much attention as an exotic magnetic order experimentally observed in kagome spin compounds [55,56] and as an origin of theoretically predicted anomalous magnetic behavior in a spin tube [57,58]. Therefore, the 1/1 Tsai-type approximant Au-Al-Gd alloy is one of the possible candidates for new magnetic phenomena associated with the cuboc order.

ACKNOWLEDGMENTS

We would like to thank R. Tamura, T. J. Sato, and T. Hiroto for fruitful discussions. This work was partly supported by Challenging Research Exploratory (Grant No. JP17K18764), Grant-in-Aid for Scientific Research on Innovative Areas (Grant No. JP19H05821). Numerical computation in this work was carried out on the Supercomputer Center at the Institute for Solid State Physics, University of Tokyo, and the supercomputers at JAEA.

APPENDIX: SPIN CONFIGURATIONS IN INCOMMENSURATE PHASES

In this Appendix, we discuss spin configurations in incommensurate phases. According to ground-state energy and its derivative with respect to the Fermi wavenumber obtained by the MC simulations (see Fig. 4 in the main text), we conclude that there are at least six incommensurate phases in $k_F \in [1.290, 1.315]$ and $[1.410, 1.535]$ Å^{-1}. Between two neighboring incommensurate phases, we find cusplike singularities in the derivative, indicating second-order transitions. Therefore, these transitions can be characterized by appropriate spin order.

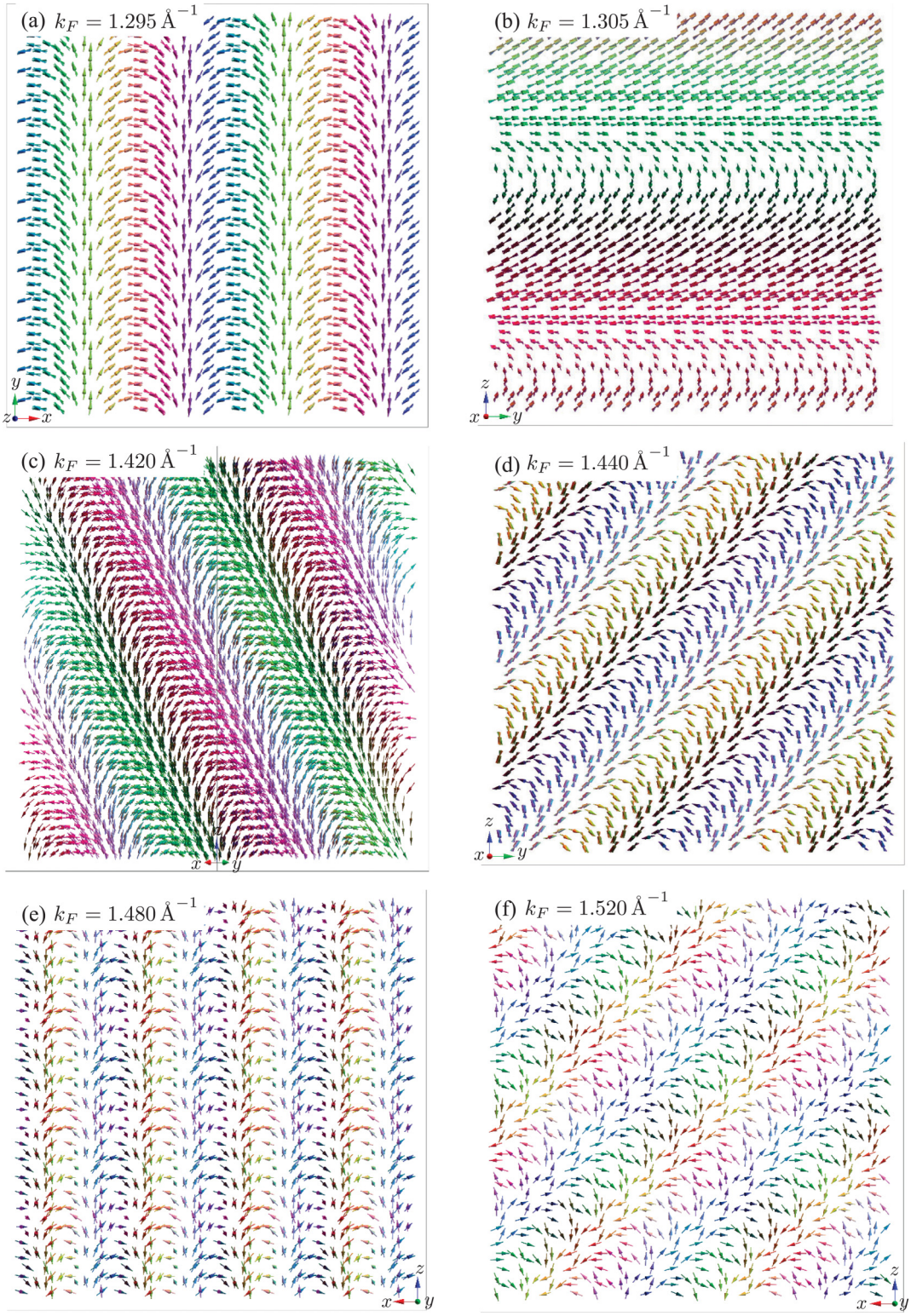

FIG. 5. Spin configurations for various Fermi wavenumbers, (a) $k_F = 1.295$, (b) 1.305, (c) 1.420, (d) 1.440, (e) 1.480, and (f) 1.520 Å^{-1}, representing the six incommensurate phases separated by cusp or jump singularities in the derivative of energy with respect to the Fermi wavenumber in Fig. 4. All of the spins in the simulated system, $N_s = 12\,288$ spins ($N_c = 8 \times 8 \times 8$ unit cells), are projected onto planes perpendicular to (a) [001], (b) [100], (c) [110], (d) [100], (e) [010], and (f) [010] axes. Spins with different directions are shown with different colors.

In order to get helpful hints for the order, we plot in Fig. 5 spin configurations for various Fermi wavenumbers representing the six incommensurate phases obtained by the MC simulations for a system with $N_s = 12\,288$ spins

($N_c = 8 \times 8 \times 8$ unit cells). All spins in the system are projected onto a plane perpendicular to a certain axis and are shown with different colors depending on their direction. Because of the projection, it is possible to have several spins on a projected position in the plane. Therefore, if one can see only one type of spin on the position, it means that spins located at the same site in each unit cell have common direction. On the other hand, the presence of several projected spins with different directions at the same position in Fig. 5 indicates that spins located at the same position in each unit cell have different directions. Based on these observations, we can judge classical orders in the system by comparing directions of spins piled up at the same position in Fig. 5.

In Figs. 5(c) and 5(e), we find several spins with different directions at the same position, while spins at the same position in Figs. 5(a), 5(b), 5(d), and 5(f) show almost the same direction. More importantly, the direction of spin rotates along one spatial direction. For instance, spins in Fig. 5(a) rotate clockwise along the x direction. This type of spin configuration is regarded as *spiral* order with a single-$\boldsymbol{q}$ vector, although the $\boldsymbol{q}$ vectors are different in each incommensurate phase [59].

Since we adopt periodic boundary condition for a finite-size system, the $\boldsymbol{q}$ vector for spiral orders is restricted to be commensurate. However, the $\boldsymbol{q}$ vector in a large system size may continuously change depending on the Fermi wavenumber. We thus conclude that the phases with spiral orders correspond to incommensurate phases in the thermodynamic limit. Based on this, we expect that phase transitions between incommensurate phases occur due to the change of the $\boldsymbol{q}$ vector.

Furthermore, in real materials, randomness due to defects and chemical disorders affects spin configurations, resulting in a disordered configuration like a spin-glass state if the randomness is strong enough, with the help of strong frustration evidenced by the presence of incommensurate states. Consequently, we consider that a part or all of incommensurate phases obtained in this study could correspond to spin-glass phases observed in Au-Al-Gd experimentally.

[1] A. P. Tsai, A. Niikura, A. Inoue, T. Masumoto, Y. Nishida, K. Tsuda, and M. Tanaka, Philos. Mag. Lett. **70**, 169 (1994).

[2] A. P. Tsai, J. Q. Guo, E. Abe, H. Takakura, and T. J. Sato, Nature (London) **408**, 537 (2000).

[3] D. Kawana, T. Watanuki, A. Machida, T. Shobu, K. Aoki, and A. P. Tsai, Phys. Rev. B **81**, 220202(R) (2010).

[4] T. Watanuki, S. Kashimoto, D. Kawana, T. Yamazaki, A. Machida, Y. Tanaka, and T. J. Sato, Phys. Rev. B **86**, 094201 (2012).

[5] K. Deguchi, S. Matsukawa, N. K. Sato, T. Hattori, K. Ishida, H. Takakura, and T. Ishimasa, Nat. Mater. **11**, 1013 (2012).

[6] G. A. Alves, M. S. Vasconcelos, and T. F. A. Alves, Phys. Rev. E **93**, 042111 (2016).

[7] K. Kamiya, T. Takeuchi, N. Kabeya, N. Wada, T. Ishimasa, A. Ochiai, K. Deguchi, K. Imura, and N. K. Sato, Nat. Commun. **9**, 154 (2018).

[8] As an experimental observation of superconductivity in approximants, see K. Deguchi, M. Nakayama, S. Matsukawa, K. Imura, K. Tanaka, T. Ishimasa, and N. K. Sato, J. Phys. Soc. Jpn. **84**, 015002 (2015); **84**, 023705 (2015).

[9] S. Watanabe and K. Miyake, Phys. Rev. Lett. **105**, 186403 (2010).

[10] S. Watanabe and K. Miyake, J. Phys.: Condens. Matter. **24**, 294208 (2012).

[11] S. Watanabe and K. Miyake, Jpn. J. Appl. Phys. **56**, 05FA01 (2017).

[12] S. Sakai, N. Takemori, A. Koga, and R. Arita, Phys. Rev. B **95**, 024509 (2017).

[13] S. Sakai and R. Arita, Phys. Rev. Res. **1**, 022002 (2019).

[14] For example, see A. P. Tsai, Chem. Soc. Rev. **42**, 5352 (2013).

[15] As a review, see A. I. Goldman, Sci. Technol. Adv. Mater. **15**, 044801 (2014).

[16] R. Tamura, Y. Muro, T. Hiroto, K. Nishimoto, and T. Takabatake, Phys. Rev. B **82**, 220201(R) (2010).

[17] M. G. Kim, G. Beutier, A. Kreyssig, T. Hiroto, T. Yamada, J. W. Kim, M. de Boissieu, R. Tamura, and A. I. Goldman, Phys. Rev. B **85**, 134442 (2012).

[18] R. Tamura, Y. Muro, T. Hiroto, H. Yaguchi, G. Beutier, and T. Takabatake, Phys. Rev. B **85**, 014203 (2012).

[19] A. Mori, H. Ota, S. Yoshiuchi, K. Iwakawa, Y. Taga, Y. Hirose, T. Takeuchi, E. Yamamoto, Y. Haga, F. Honda, R. Settai, and Y. Ōnuki, J. Phys. Soc. Jpn. **81**, 024720 (2012).

[20] P. Das, P.-F. Lory, R. Flint, T. Kong, T. Hiroto, S. L. Bud'ko, P. C. Canfield, M. de Boissieu, A. Kreyssig, and A. I. Goldman, Phys. Rev. B **95**, 054408 (2017).

[21] T. Hiroto, G. H. Gebresenbut, C. P. Gómez, Y. Muro, M. Isobe, Y. Ueda, K. Tokiwa, and R. Tamura, J. Phys.: Condens. Mater. **25**, 426004 (2013).

[22] T. Hiroto, K. Tokiwa, and R. Tamura, J. Phys.: Condens. Mater. **26**, 216004 (2014).

[23] G. H. Gebresenbut, M. S. Andersson, P. Beran, P. Manuel, P. Nordblad, M. Sahlberg, and C. P. Gómez, J. Phys.: Condens. Mater. **26**, 322202 (2014).

[24] A. Ishikawa, T. Hiroto, K. Tokiwa, T. Fujii, and R. Tamura, Phys. Rev. B **93**, 024416 (2016).

[25] G. H. Gebresenbut, M. S. Andersson, P. Nordblad, M. Sahlberg, and C. P. Gómez, Inorg. Chem. **55**, 2001 (2016).

[26] A. Ishikawa, T. Fujii, T. Takeuchi, T. Yamada, Y. Matsushita, and R. Tamura, Phys. Rev. B **98**, 220403(R) (2018).

[27] T. J. Sato, A. Ishikawa, A. Sakurai, M. Hattori, M. Avdeev, and R. Tamura, Phys. Rev. B **100**, 054417 (2019).

[28] S. Yoshida, S. Suzuki, T. Yamada, T. Fujii, A. Ishikawa, and R. Tamura, Phys. Rev. B **100**, 180409(R) (2019).

[29] K. Fukamichi, T. Masumoto, M. Oguchi, A. Inoue, T. Goto, T. Sakakibara, and S. Todo, J. Phys. F: Met. Phys. **16**, 1059 (1986).

[30] W. W. Warren, H.-S. Chen, and G. P. Espinosa, Phys. Rev. B **34**, 4902 (1986).

[31] Y. Hattori, A. Niikura, A. P. Tsai, A. Inoue, T. Masumoto, K. Fukamichi, H. Aruga-Katori, and T. Goto, J. Phys.: Condens. Matter. **7**, 2313 (1995).

[32] B. Charrier and D. Schmitt, J. Magn. Magn. Mater. **171**, 106 (1997); **189**, 165 (1998).

[33] D. R. Noakes, G. M. Kalvius, R. Wäppling, C. E. Stronach, M. F. White, Jr., H. Saito, and K. Fukamichi, Phys. Lett. A **238**, 197 (1998).
[34] Z. Islam, I. R. Fisher, J. Zarestky, P. C. Canfield, C. Stassis, and A. I. Goldman, Phys. Rev. B **57**, R11047 (1998).
[35] T. J. Sato, H. Takakura, A. P. Tsai, and K. Shibata, Phys. Rev. Lett. **81**, 2364 (1998).
[36] T. J. Sato, H. Takakura, A. P. Tsai, K. Shibata, K. Ohoyama, and K. H. Andersen, Phys. Rev. B **61**, 476 (2000).
[37] M. Scheffer, M. Rouijaa, J. B. Suck, R. Sterzel, and R. E. Lechner, Mat. Sci. Eng. **294-296**, 488 (2000).
[38] M. A. Ruderman and C. Kittel, Phys. Rev. **96**, 99 (1954).
[39] T. Kasuya, Prog. Theor. Phys. **16**, 45 (1956).
[40] K. Yosida, Phys. Rev. **106**, 893 (1957).
[41] Y. Achiam, T. C. Lubensky, and E. W. Marshall, Phys. Rev. B **33**, 6460 (1986).
[42] C. Godrèche, J. M. Luck, and H. Orland, J. Stat. Phys. **45**, 777 (1986).
[43] Y. Okabe and J. Niizeki, J. Phys. Soc. Jpn. **57**, 16 (1988).
[44] D. Ledue, J. Teillet, J. Carnet, and J. Dujardin, J. Non-Cryst. Solids **153**, 403 (1993).
[45] E. Y. Vedmedenko, H. P. Oepen, and J. Kirschner, Phys. Rev. Lett. **90**, 137203 (2003).
[46] R. Lifshitz, Phys. Rev. Lett. **80**, 2717 (1998); Mater. Sci. Eng. A **294-296**, 508 (2000); also see Rev. Mod. Phys. **69**, 1181 (1997).
[47] S. Wessel, A. Jagannathan, and S. Haas, Phys. Rev. Lett. **90**, 177205 (2003).
[48] A. Jagannathan, Phys. Rev. Lett. **92**, 047202 (2004); Phys. Rev. B **71**, 115101 (2005).
[49] S. Thiem and J. T. Chalker, Eur. Phys. Lett. **110**, 17002 (2015); Phys. Rev. B **92**, 224409 (2015).
[50] T. Sugimoto, T. Tohyama, T. Hiroto, and R. Tamura, J. Phys. Soc. Jpn. **85**, 053701 (2016).
[51] The cutoff range R_c should be much larger than the mean free path of conduction electrons. In Au-Al-Gd, the mean free path is estimated to be the length of the lattice unit from the electric conductivity (R. Tamura, private communication) and thus our R_c satisfies the condition. In addition, $R_c = 50$ Å is long enough to get convergence, since the difference of the total sum of exchange energy for all possible spins between $R_c = 50$ and 60 Å is less than 6×10^{-5} J.
[52] J.-C. Domenge, P. Sindzingre, C. Lhuillier, and L. Pierre, Phys. Rev. B **72**, 024433 (2005).
[53] J.-C. Domenge, C. Lhuillier, L. Messio, L. Pierre, and P. Viot, Phys. Rev. B **77**, 172413 (2008).
[54] L. Messio, C. Lhuillier, and G. Misguich, Phys. Rev. B **83**, 184401 (2011).
[55] H. Ishikawa, T. Okubo, Y. Okamoto, and Z. Hiroi, J. Phys. Soc. Jpn. **83**, 043703 (2014).
[56] B. Fåk, E. Kermarrec, L. Messio, B. Bernu, C. Lhuillier, F. Bert, P. Mendels, B. Koteswararao, F. Bouquet, J. Ollivier, A. D. Hillier, A. Amato, R. H. Colman, and A. S. Wills, Phys. Rev. Lett. **109**, 037208 (2012).
[57] K. Seki and K. Okunishi, Phys. Rev. B **91**, 224403 (2015).
[58] M. Ochiai, K. Seki, and K. Okunishi, J. Phys. Soc. Jpn. **86**, 114701 (2017).
[59] The spin configuration in Fig. 5(f) seems different from the others, indicating not a simple spiral order. The spin vectors look undulating rather than rotating, which may imply a multiple-$\boldsymbol{q}$ state such as a skyrmion lattice [e.g., see N. Nagaosa and Y. Tokura, Nat. Nanotechnol. **8**, 899 (2013)]. Nevertheless, an incommensurate phase is expected in the thermodynamic limit as is the case for other single-$\boldsymbol{q}$ states.